Acta Cryst B
STRUCTURAL SCIENCE
CRYSTAL ENGINEERING
MATERIALS
ISSN 2052-5206

Ab initio structure determination of $[Eu_5(C_2H_4O_2)_6(CH_3CO_2)_3]_n$ by X-ray powder diffraction

Amal Abdallah,[a] Souad Ammar,[a] Voraksmy Ban,[b] Romain Sibille[c] and Michel Francois[d]*

[a]Université Paris Diderot, SPC, CNRS (UMR 7086), ITODYS, 15 rue Jean Antoine de Baïf, Paris, 75205, France, [b]Laboratory for Condensed Matter Research, Paul Scherrer Institut, Villigen, 5232, Switzerland, [c]Laboratory for Neutron Scattering and Imaging, Paul Scherrer Institut, Villigen, 5232, Switzerland, and [d]Université de Lorraine, CNRS (UMR 7198), IJL, BP 70239, Nancy, 54000, France. *Correspondence e-mail: michel.francois@univ-lorraine.fr

Received 2 August 2018
Accepted 13 September 2018

Edited by R. Černý, University of Geneva, Switzerland

Keywords: crystal structure; MOF; trivalent europium; metal glycolate.

CCDC reference: 1867704

Supporting information: this article has supporting information at journals.iucr.org/b

The compound $[Eu_5(C_2H_4O_2)_6(CH_3CO_2)_3]_n$ was synthesized by dissolving acetate europium salt in ethylene glycol solvent and heating under reflux for a short time. Its structure was solved *ab initio* from synchrotron powder diffraction data using optimization methods in direct space. The compound has a very large unit-cell volume of 23679 Å^3 and the highest centred cubic symmetry space group, $Ia\bar{3}d$ (No. 230). The porous metal–organic framework structure is similar to those usually observed in zeolites, with pores volumes of 82 Å^3, which is of potential interest for gas storage.

1. Introduction

Nowadays, metal–glycolate solids are considered for different purposes. They are mostly prepared and investigated as solid intermediates in the preparation of chemically, structurally and microstructurally controlled oxide particles (Takase *et al.*, 2017; Das *et al.*, 2009; Ksapabutr *et al.*, 2004; Pan *et al.*, 2015; Day *et al.*, 1996; Ng *et al.*, 2008; Yu *et al.*, 2007 Baklanova *et al.*, 2014) or metal (Chakroune *et al.*, 2005; Abdallah *et al.*, 2015; Takahashi *et al.*, 2016; Anžlovar *et al.*, 2008), but they are also studied as intrinsic functional materials, taking advantage of the versatility of their crystalline structure, their lightness and, of course, the variety of their own physico-chemical properties. Typically, some of them, owing to the magnetic properties of their constitutive metal cations, exhibit interesting magnetocaloric properties at low temperature making them valuable for cryogenic magneto-refrigeration applications (Abdallah *et al.*, 2019; Chen *et al.*, 2014). Others, owing to the chelating properties of their organic component, namely glycolate ligands, allow a better reactivity in certain catalytic reactions, such as those involved in the polycondensation of ethylene glycol with bis-(hydroxyethyl)terephthalate for the production of poly(ethylene terephthalate) (PET) – an important thermoplastic material (Biros *et al.*, 2002). In other cases, their open crystallographic structure as metal–organic frameworks (MOFs) allow their use for different gas storage or separation applications (Wasson *et al.*, 2009). These examples are, of course, not exhaustive and the chemical richness of this class of molecular materials is not yet completely explored. Investigations on new compounds with original properties are still in progress. This growing interest is favoured by the great ease of producing these materials. Usually, they are obtained by dissolving metallic salts in a glycol solvent (1,2-ethanediol, 1,4-

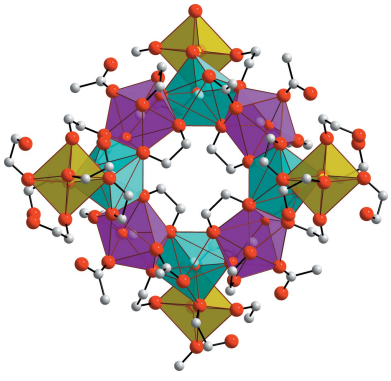

butanediol, glycerol, diethylene glycol, triethylene glycol, *etc.*) and heating up the mixture up to the boiling point of the solvent for a few minutes. Hybrid compounds are immediately formed and precipitate. They are also readily recovered by centrifugation and, once dried in air, do not require specific storage conditions.

Focusing on the structure of these materials, the coordination possibilities offered by glycolate molecules (bridging, chelating and terminal modes) (Hubert-Pfalzgraf, 1998) allow the construction of more or less interconnected metal polyhedra within different lattice dimensionalities (zero-, one-, two- or three-dimensional). Depending on the organic linkers, different spatial arrangements can thus be achieved and structures based on isolated nanoclusters, chains, layers or three-dimensional polymers, including three-dimensional lattices containing shape-controlled cages, can be obtained. The nature of the metal cation is also important in this architectural design, and particularly its ability to be coordinated to several hetero-atoms. In particular, lanthanide cations are known to favour the formation of polyhedra with high coordination number. Moreover, these cations, owing to their 4*f* valence electrons, possess various magnetic and optical properties, leading to additional functionalities.

In this context, we were interested in producing europium-based glycolate solids and in elucidating their structure using synchrotron radiation, to enable an evaluation of their potential as functional materials in relation to their chemical composition and/or crystallographic structure. To assist our structural characterizations, thermogravimetry and Eu Mossbauer spectroscopy were performed.

2. Experimental

2.1. Synthesis and crystallization

Europium(III) acetate hydrate (99.99%, Aldrich) and 1,2-ethanediol, commonly called ethylene glycol and abbreviated here as egH_2 (99%, Acros Organic), were purchased and used without further purification. In practice, 3 mmol of metallic salts were dissolved in 125 ml of egH_2. The reaction solution was heated (6°C min^{-1}) up to reflux at 195°C for 2 h under mechanical stirring. The solid formed at the boiling temperature was a beige powder. After cooling down to room temperature, the solid was recovered by centrifugation and then washed three times with ethanol before being dried and stored under primary vacuum. Infrared spectroscopy performed on the dried powder using the KBr technique, confirmed its acetato-glycolate composition (see Fig. S1 in the supporting information), allowing us to hypothesize that the hybrid material formed contains europium, ethylene glycol (or ethylene glycolate) and acetate species.

2.2. Data collection and indexing

X-ray diffraction data were collected at room temperature at the Swiss Light Source (SLS) synchrotron using the Materials Science beamline X04SA (Willmott *et al.*, 2013). The wavelength of 0.77665 (2) Å was calibrated with standard NIST silicon. The powder sample was measured in a glass capillary (ø = 0.4 mm) with Debye–Scherrer geometry using a MYTHEN II rapid multistrip detector (Bergamaschi *et al.*, 2010). In order to cover blind zones of the detector, diffraction patterns have been measured at four different detector positions (about 10 seconds per position), which were then averaged. Intensity data were collected up to 60° (2θ) with a step of 0.0036°.

Twenty reflections between 3 and 16° (2θ) were chosen with the graphic interface of *WinPlotr* in *FullProf Suite* (Rodríguez-Carvajal, 1993) to be indexed with the *Dicvol06* (Louër & Boultif, 2007) program. The whole pattern was indexed in a cubic lattice with a relatively large parameter a = 28.707 Å (V = 23657.4 Å^3) and a figure of merit M_{20} = 42.8.

Successive Lebail refinement and space group verification identified two possible space groups, $Ia\bar{3}d$ (No. 230) and $I\bar{4}3d$ (No. 220), with very close values of goodness-of-fit (1.95 and 1.92, respectively). Accurate examination of the pattern shows that the intensity of the (310) reflection at 2θ = 4.904° is zero, indicating a systematic extinction condition in the (hk0) reflections with $k \neq 2n$ and $l \neq 2n$ consistent with $Ia\bar{3}d$ which was used in all subsequent analysis and discussion.

2.3. Structure solution

The search for a starting structural model was conducted by global optimization in direct space with the *FOX* (Favre-Nicolin & Černý, 2002) program and using a parallel tempering algorithm. The ethylene glycol and acetate species were assumed as fully deprotonated and are abbreviated as eg^{2-} ($^-OC_2H_4O^-$) and ac^- ($CH_3CO_2^-$), respectively. The input models of these anions were defined by describing the two molecules in terms of Fenske–Hall Z-matrix format without H atoms. For eg^{2-}, the dihedral angles O—C—C—O were defined as intramolecular degrees of freedom and varied during the optimization. Three Wyckoff positions for the Eu atoms were identified, Eu1 (96*h*), Eu2 (48*g*) and Eu3 (16*a*). As europium cations are presumably trivalent in this type of compound, two hypotheses verifying the electroneutrality were then formulated for the unit formula (Z = 32) including the organic components: (i) $Eu^{3+}{}_5(eg^{2-})_6(ac^-)_3$ and (ii) $Eu^{3+}{}_5(eg^{2-})_3(ac^-)_9$, corresponding to theoretical organic weight content of 32.2 and 40.2%, respectively. ^{151}Eu Mossbauer spectrometry performed at room and liquid nitrogen temperatures confirmed the trivalent valence state of Eu cations in our compound (see Fig. S2 in the supporting information). The thermogravimetry analysis performed in air from 25 to 600°C showed a total organic weight loss of 36.39 wt%, which is much more compatible with the first formula hypothesis than with the second one (Fig. S3 in the supporting information). The formula $Eu^{3+}{}_5(eg^{2-})_6(ac^-)_3$ was thus retained for the rest of this article. The calculated density is 2.838 g cm^{-3}, which is very reasonable for this kind of molecular solid.

In summary, the model contains three sites for Eu atoms, Eu1 (96*h*), Eu2 (48*g*), Eu3 (16*a*), and three independent molecules in general position: two ethylene glycolate denoted

Table 1
Experimental details.

Crystal data	
Chemical formula	$C_{18}H_{33}Eu_5O_{18}$
M_r	1297.29
Crystal system, space group	Cubic, $Ia\bar{3}d$
Temperature (K)	293
a (Å)	28.7121 (3)
V (Å^3)	23669.7 (4)
Z	32
Radiation type, wavelength (Å)	Synchrotron, λ = 0.776651
μ (mm^{-1})	13.20
Specimen shape, length × diameter (mm)	Cylinder, 10.0 × 0.5
Data collection	
Diffractometer	CRISTAL Beamline, SOLEIL
Specimen mounting	Powder in a glass capillary
Data collection mode	Transmission
Scan method	Step
2θ values (°)	$2\theta_{min}$ = 2.01, $2\theta_{max}$ = 60.01, $2\theta_{step}$ = 0.0036
Refinement	
R factors and goodness-of-fit	R_p = 0.026, R_{wp} = 0.029, R_{exp} = 0.004, R_{Bragg} = 0.076, χ^2 = 4637.610
No. of parameters	53
No. of restraints	16
H-atom treatment	H-atom parameters not refined

Computer programs: *FOX* (Favre-Nicolin & Černý, 2002), *FullProf* (Rodriguez-Carvajal, 1993), *DIAMOND* (Brandenburg & Putz, 1999).

eg_A and eg_B and one acetate denoted ac (see Fig. S4 in the supporting information). The lattice contains 160 Eu trivalent cations, 192 ethylene glycolate and 96 acetate anions, corresponding to the $Eu_5(eg)_6(ac)_3$ formula unit with 32 formula per unit cell.

The coordinates of Eu2 and Eu3 sites were fixed to the values found during the previous optimizations. The position and orientation of the three independent molecules eg_A, eg_B and ac quickly converged and very satisfactory values of R_p and R_{wp} close to 0.04 were obtained. The model was then refined by the Rietveld method, using *FullProf* (Rodríguez-Carvajal, 1993).

2.4. Rietveld refinement

Rietveld refinements were performed by fixing, at the beginning, all the profile parameters to the values given by the Lebail decomposition. The position of C and O atoms of eg and ac anions were refined, with the constraints explained hereafter. The structure model contains 15 atomic positions (except atoms H): three for the Eu atoms and 12 (six sites for C and six sites for O) for the three molecules eg_A, eg_B and ac. Forty seven parameters depending on the intensity were released first: one scaling factor, 40 atomic coordinates (four for Eu – three for Eu1 and one for Eu2, 18 for C and 18 for O atoms) and six temperature factors (one for every Eu site and one for each molecule type). Also, ten distances and seven angular restraints were applied to respect the geometry of eg_A, eg_B and ac molecules. Typically, the C—C and C—O distances were constrained to be 1.48 (1) and 1.43 (1) Å, respectively, in both eg_A and eg_B molecules. Also, the O—C—C angle in these molecules was fixed to 109.5 (2)°. The C—C distance and the C—C—O angle in the ac molecule were constrained to 1.54 (1) Å and 120.0°, respectively. The H atoms of eg^{2-} and ac^- molecules (11 H positions) were positioned geometrically but not refined. Finally, all the intensity and profile parameters were released (53 parameters among which 47 intensity and six profile parameters).

The refinement converges satisfactorily with R_{Bragg} = 0.076, R_{wp} = 0.030 and R_p = 0.026; the refined parameters are listed in Table 1. The final Rietveld plot is given in Fig. 1. The atomic coordinates and temperature factors are reported in Table S1 in the supporting information.

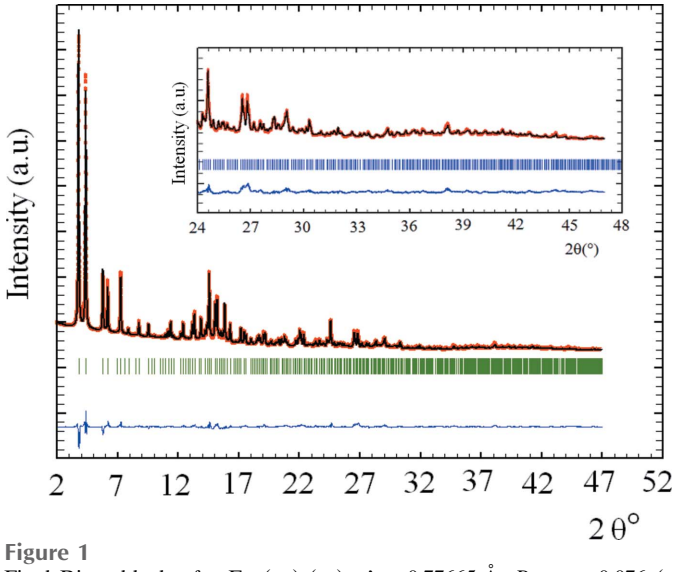

Figure 1
Final Rietveld plot for $Eu_5(eg)_6(ac)_3$, λ = 0,77665 Å. R_{Bragg} = 0.076 (a zoom is in the inset). Observed intensities are indicated by dots, the best-fit profile (upper trace) and the difference pattern (lower trace) are solid lines. The vertical bars correspond to the positions of the Bragg peaks.

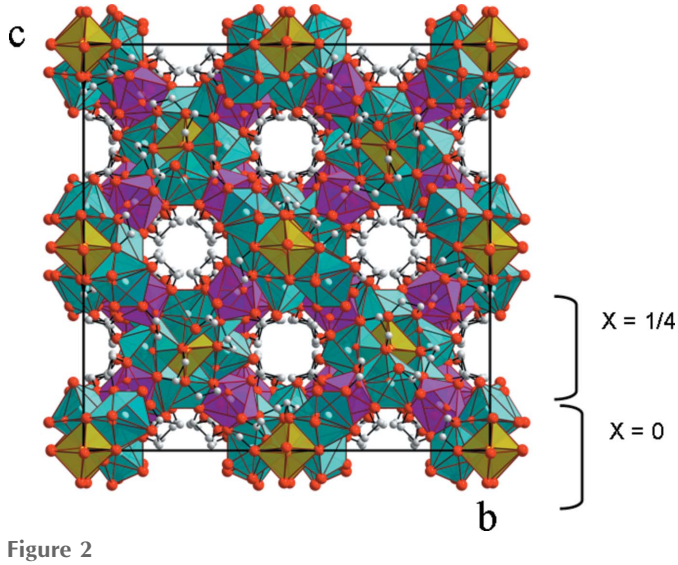

Figure 2
General view of $Eu_5(eg)_6(ac)_3$ structure. Projection along the a axis. $[Eu1O_7]^{11-}$, $[Eu2O_8]^{13-}$ and $[Eu3O_6]^{9-}$ polyhedra appear in cyan, purple and yellow, respectively. H atoms are omitted for clarity.

Table 2
Selected geometric parameters (Å, °) for $Eu_5(eg)_6(Ac)_3$.

Eu1—O4^{i}	2.487 (12)	Eu3—O14^{vii}	2.394 (11)
Eu1—O5^{ii}	2.381 (11)	Eu3—O14^{viii}	2.394 (9)
Eu1—O8	2.355 (12)	Eu3—O14^{ix}	2.394 (11)
Eu1—O14^{iii}	2.620 (11)	Eu3—O14^{x}	2.394 (11)
Eu1—O14^{iv}	2.737 (9)	Eu3—O14^{xi}	2.394 (9)
Eu1—O15	2.610 (11)	Eu3—O14^{xii}	2.394 (11)
Eu1—O15^{iv}	2.320 (12)	C2—C3	1.502 (15)
Eu2—O4^{v}	2.229 (12)	C2—O5	1.409 (13)
Eu2—O4^{ii}	2.230 (12)	C3—O4	1.439 (18)
Eu2—O5^{v}	2.380 (9)	C6—C7	1.545 (17)
Eu2—O5^{ii}	2.380 (9)	C7—O8	1.33 (2)
Eu2—O9	2.287 (14)	C7—O9	1.38 (2)
Eu2—O9^{vi}	2.287 (13)	C12—C13	1.493 (17)
Eu2—O15	2.672 (10)	C12—O15	1.479 (16)
Eu2—O15^{vi}	2.672 (11)	C13—O14	1.488 (16)
O5···O15^{xiii}	2.608 (15)		
C3—C2—O5	105.5 (12)	O8—C7—O9	121.2 (18)
C2—C3—O4	113.9 (15)	C13—C12—O15	105.9 (15)
C6—C7—O8	117.1 (17)	C12—C13—O14	108.3 (13)
C6—C7—O9	121.4 (18)		

Symmetry codes: (i) $-y+\frac{1}{4}, x+\frac{3}{4}, z+\frac{1}{4}$; (ii) $-z+1, -x+1, -y+1$; (iii) $y-1, z, x+1$; (iv) $-z+1, -x+1, -y+2$; (v) $-x+\frac{1}{4}, -z+\frac{7}{4}, y+\frac{3}{4}$; (vi) $y-\frac{3}{4}, x+\frac{3}{4}, -z+\frac{7}{4}$; (vii) $x, y-1, z-1$; (viii) $y-1, z-1, x$; (ix) $z-1, x, y-1$; (x) $-x, -y+1, -z+1$; (xi) $-y+1, -z+1, -x$; (xii) $-z+1, -x, -y+1$; (xiii) $-y+1, -z+1, -x+1$.

3. Results and discussion

3.1. General description of the structure

A polyhedral representation of the structure is given in Fig. 2. The structure forms a three-dimensional network of cages and channels, usually observed in zeolite-type compounds similar to numerous other MOFs (Smaldone *et al.*, 2010). The volume of the accessible voids calculated by the crystallographic software *PLATON* (Spek, 2009) when all H atoms are geometrically positioned into the structure is estimated to be around 82 Å^3.

3.2. Europium coordination and valence

The environment of the Eu1, Eu2 and Eu3 europium sites is represented in Fig. 3 and the Eu—O distances are reported in Table 2. The coordination number (CN) of all these europium sites is found to be 7, 8 and 6, respectively.

Eu1 (96*h*) has seven O atoms as first neighbours, four from bridging eg_A and eg_B molecules (O4, O5, O14, O15), two from a chelating eg_B molecule (O14, O15) and one from a bridging ac (O8). The Eu—O distances range between 2.320 (12) and 2.737 (9) Å. Eu2 (48*g*) is coordinated to eight O atoms, four from two chelating eg_A (2 × O4, 2 × O5), two from two bridging eg_B (2 × O5) and two from bridging ac (2 × O9). The Eu2—O distances range from 2.229 (12) to

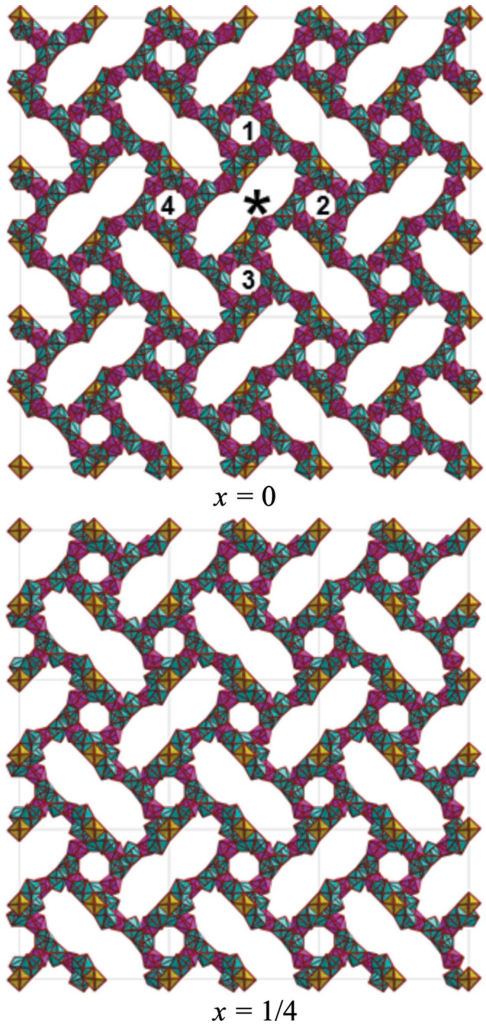

Figure 4
Polyhedral representation of $[Eu1O_7]^{11-}$ (cyan), $[Eu2O_8]^{13-}$ (purple) and $[Eu3O_6]^{9-}$ (yellow) in slabs at $x = 0$ and $\frac{1}{4}$.

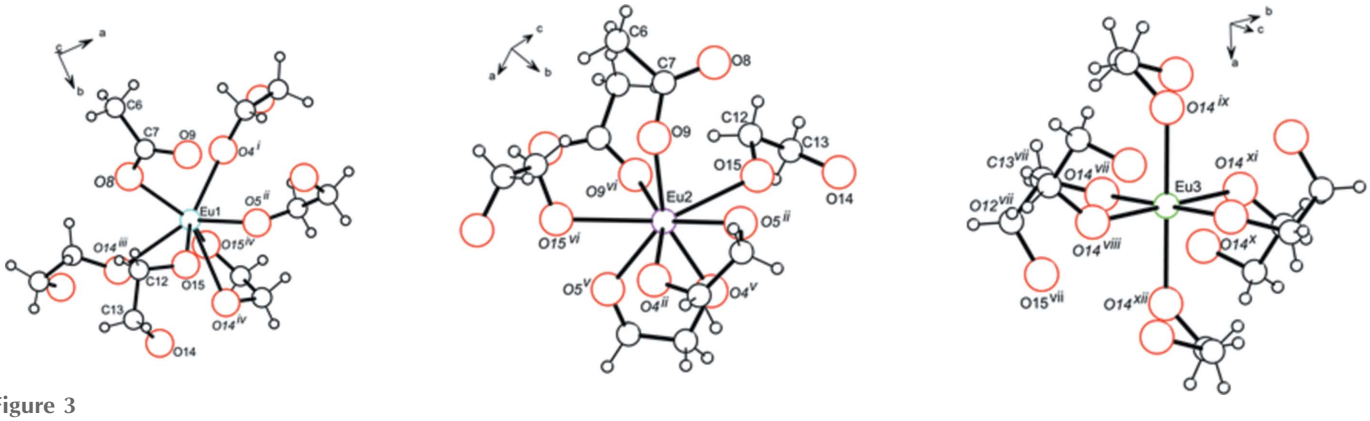

Figure 3
Eu1 (CN = 7), Eu2 (CN = 8) and Eu3 (CN = 6) site environments in $Eu_5(eg)_6(ac)_3$ crystal. Symmetry codes are given in Table 2.

2.672 (11) Å. Eu3 (16*a*) has a regular octahedral O atom environment [Eu—O = 2.394 (11) Å] with O atoms coming from six bridging eg_B (6 × O14) anions. Comparison with Eu—O bond valence calculations indicate that Eu atoms are trivalent, in agreement with ^{151}Eu Mossbauer spectroscopy analysis. Moreover, observed Eu—O distances in $Eu_5(eg)_6(ac)_3$ are in agreement with similar distances found in numerous Eu^{III}-based organo–metallic crystal structures reported in the CCDC database (Rau, 1966; Phanon & Gautier-Luneau, 2010; Barja *et al.*, 2003; Hu *et al.*, 1999).

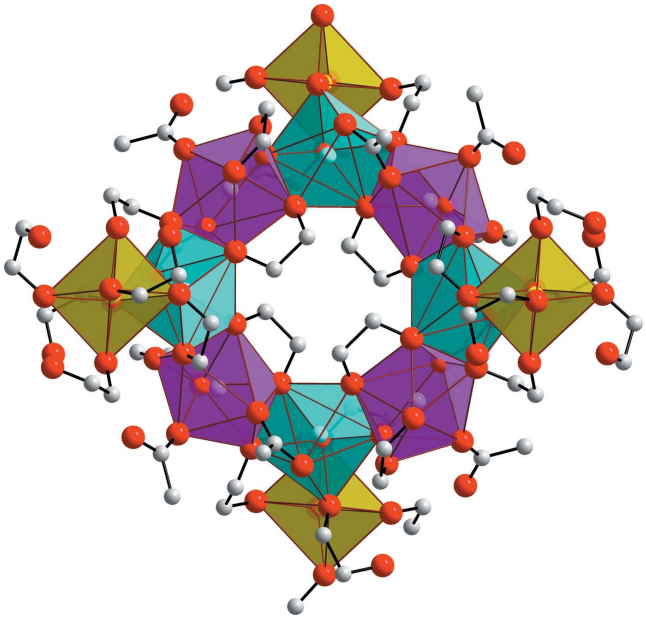

Figure 5
Representation of the ring formed by the eight europium coordination polyhedra ($[Eu1O_7]^{11-}$ and $[Eu2O_8]^{13-}$ alternately) sharing edges in the (*b*,*c*) plane of $Eu_5(eg)_6(ac)_3$ structure. Four $[Eu3O_6]^{9-}$ octahedra are connected to each ring, by sharing edges. H atoms have been omitted for clarity and the $[Eu1O_7]^{11-}$, $[Eu2O_8]^{13-}$ and $[Eu3O_6]^{9-}$ octahedra have been drawn in cyan, purple and yellow, respectively.

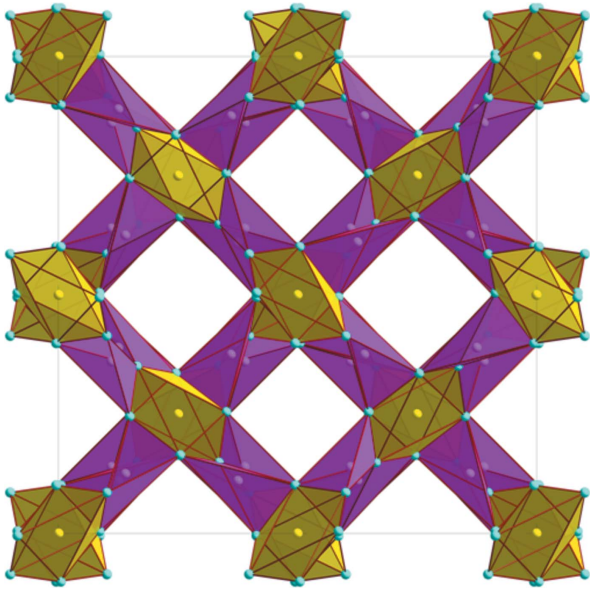

Figure 6
Europium sub-network projection along the *b* axis with the representation of Eu1-based tetrahedra in purple and Eu1-based pseudo-hexagons in yellow.

3.3. Connection of the coordination polyhedra

To understand in more detail this complicated structure, one has to imagine that it may be decomposed in two layers, 1 and 2, corresponding to slabs at $x = 0$ and $x = \frac{1}{4}$, respectively (Fig. 2). In the first layer ($x = 0$) or the second layer ($x = \frac{1}{4}$), it is emphasized that the connection of polyhedra leads to the formation of rings. Thus, rings constituted by eight polyhedra sharing edges, alternately $[Eu1O_7]^{11-}$ and $[Eu2O_8]^{13-}$, can be distinguished in the (*b*,*c*) plane (Fig. 4). A polyhedral representation of these rings is given in Fig. 5. Around these rings, four small rings (denoted 1–4), interconnected by a bridge of three polyhedra, $[Eu1O_7]^{11-}$, $[Eu2O_8]^{13-}$ and $[Eu3O_6]^{9-}$, can

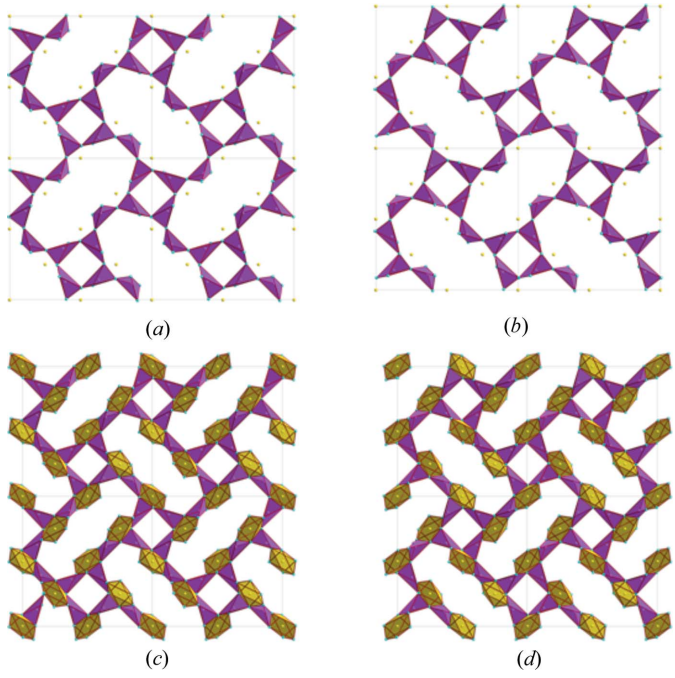

Figure 7
Europium sub-network viewed along the *a* axis (*a*) slab 1 ($x = 0$) and (*b*) slab 2 ($x = \frac{1}{4}$) and the same sub-network including the Eu1-based hexagons (*c*) slab 1 ($x = 0$) and (*d*) ($x = \frac{1}{4}$).

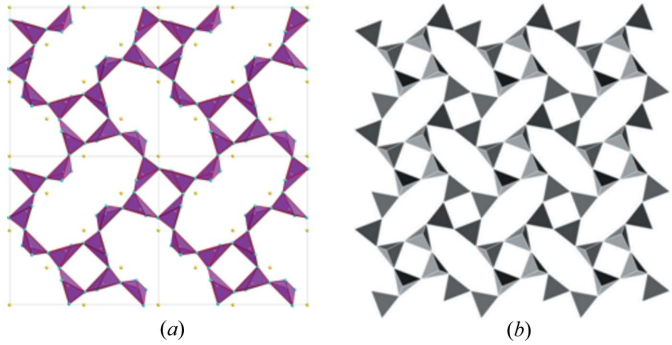

Figure 8
Tetrahedral sub-network $Eu2[(Eu1)_4]^{15+}$ in $Eu_5(eg)_6(ac)_3$ (*a*) compared with that commonly observed between $[SiO_4]^{4-}$ in phyllosilicate (*b*).

be seen (Fig. 4, left view), providing a large space, denoted *. The second layer ($x = \frac{1}{4}$) can be described by translating the first layer ($x = 0$) along the $\frac{1}{2}$**b** or $\frac{1}{2}$**c** vectors.

3.4. Europium sub-network

The projection of the europium sub-network along the *b* axis is represented in Fig. 6 and shows that europium atoms Eu2 (48*g*) occupy the centre of very deformed tetrahedra formed by four Eu1 atoms, in which the Eu1–Eu2 distances range from 3.684 to 3.786 Å. The Eu2–Eu2 distance between two tetrahedra is 6.825 Å. Eu3 atoms (16*a*) are at the centre of a pseudo-hexagon formed by six Eu1 atoms, four Eu1 atoms are in the same plane and two opposite Eu1 atoms deviate 0.4 Å from the plane. The six Eu3—Eu1 distances are identical and equal to 3.808 (3) Å. This value is equivalent to the metal–metal distance commonly measured in hybrid compounds containing Eu atoms and oxygen-based ligands, such as carboxylates, acting as organic linkers (3.8 Å) (Zhang *et al.*, 2017; Feng *et al.*, 2016; Sun *et al.*, 2016).

This sub-network also can be decomposed into slices along the *a* axis (Fig. 7). The connection of the pseudo-tetrahedral motifs in the three directions agrees with the three-dimensional character of the structure. In a representative slice, each Eu1-based tetrahedron shares two or three corners in the connections in the (*b*,*c*) plane, while it shares its remaining free corners for the connection out of the (*b*,*c*) plane. Slices (*b*,*c*) at $x = 0$ and $x = \frac{1}{4}$ can be superimposed by a translation of $\frac{1}{2}$**b** and $\frac{1}{2}$**c**, respectively.

Interestingly, this organization of Eu1-based tetrahedra in the $Eu_5(eg)_6(ac)_3$ crystal is similar to that commonly observed between $[SiO_4]^{4-}$ tetrahedral units in phyllosilicates (Brown & Nadeau, 1984) as illustrated in Fig. 8.

In summary, the cubic compound $Eu_5(eg)_6(ac)_3$ ($Ia\bar{3}d$) has a metallic skeleton made of trivalent europium centres. The architecture of this metallic sub-network provides holes and tunnels running along the three crystallographic directions. The general architecture of this structure is reminiscent of those usually encountered in zeolite-type compounds, with an $[Eu2(Eu1)_4]$-based skeleton similar to that observed in phyllosilicates (Brown & Nadeau, 1984).

The average volume of the voids forming the structure of the polyol-made $Eu_5(eg)_6(ac)_3$ crystals is estimated to be about 82 $Å^3$, which is large enough to host small molecules, such as dihydrogen (H_2) making these materials potentially valuable for gas storage applications.

4. Related literature

References cited in the supporting information include: Nakamoto (1993) and Knetsch & Groeneveld (1973*a*,*b*).

References

Abdallah, A., Gaudisson, T., Sibille, R., Nowak, S., Cheikhrouhou-Koubaa, W., Shinoda, K., François, M. & Ammar, S. (2015). *Dalton Trans.* **44**, 16013–16023.

Abdallah, A., Nowak, S., Cheikhrouhou-Koubaa, W., Sibille, R., Ban, V., François, M. & Ammar, S. (2019). In preparation.

Anžlovar, A., Orel, Z. C. & Žigon, M. (2008). *J. Nanosci. Nanotechnol.* **8**, 3516–3525.

Barja, B., Aramendia, P., Baggio, R., Garland, M. T., Pena, O. & Perec, M. (2003). *Inorg. Chem. Acta*, **355**, 183–109.

Baklanova, I. V., Krasil'nikov, V. N., Zhukov, P., Gyrdasova, O. I., Perelyaeva, L. A., Buldakova, L. Y., Yanchenko, M. Y. & Shein, I. R. (2014). *Russ. J. Inorg. Chem.* **59**, 29–33.

Bergamaschi, A., Cervellino, A., Dinapoli, R., Gozzo, F., Henrich, B., Johnson, I., Kraft, P., Mozzanica, A., Schmitt, B. & Shi, X. (2010). *J. Synchrotron Rad.* **17**, 653–668.

Biros, S. M., Bridgewater, B. M., Villeges-Estrada, A., Tanski, J. M. & Parkin, G. (2002). *Inorg. Chem.* **41**, 4051–4057.

Brandenburg, K. & Putz, H. (1999). *DIAMOND*. Crystal Impact GbR, Bonn, Germany.

Brown, G. & Nadeau, P. (1984). *Philos. Trans. R. Soc. A*, **311**, 221–240.

Chakroune, N., Viau, G., Ammar, S., Jouini, N., Gredin, P., Vaulay, M.-J. & Fiévet, F. (2005). *New J. Chem.* **29**, 355–361.

Chen, Y.-C., Guo, F.-S., Liu, J.-L., Leng, J.-D., Vrábel, P., Orendáč, M., Prokleška, J., Sechovský, V. & Tong, M.-L. (2014). *Chem. Eur. J.* **20**, 3029–3035.

Das, J., Evans, I. R. & Khushalani, D. (2009). *Inorg. Chem.* **48**, 3508–3510.

Day, V. W., Eberspacher, T. A., Frey, M., Klemperer, W. G., Liang, S. & Payne, D. A. (1996). *Chem. Mater.* **8**, 330–332.

Favre-Nicolin, V. & Černý, R. (2002). *J. Appl. Cryst.* **35**, 734–743.

Feng, X., Sun, Y.-L., Li, R.-F., Zhang, T., Guo, N. & Wang, L.-Y. (2016). *Inorg. Chem. Commun.* **73**, 190–195.

Hu, M.-L., Huang, Z.-Y., Cheng, Y.-Q., Wang, S., Lin, J.-J., Hu, Y., Xu, D.-J., Xu, Y.-Z. (1999). *Chin. J. Chem.* **17**, 637–643.

Hubert-Pfalzgraf, L. G. (1998). *Coord. Chem. Rev.* **178–180**, 967–997.

Knetsch, D. & Groeneveld, W. L. (1973*a*). *Inorg. Chim. Acta*, **7**, 81–87.

Knetsch, D. & Groeneveld, W. L. (1973*b*). *Recl Trav. Chim. Pays-Bas*, **92**, 855–864.

Ksapabutr, B., Gulari, E. & Wongkasemjit, S. (2004). *Mater. Chem. Phys.* **83**, 34–42.

Louër, D. & Boultif, A. (2007). *Z. Kristallogr. Suppl.* **26**, 191–196.

Ng, S.-H., Chew, S.-Y., dos Santos, D. I., Chen, J., Wang, J.-Z., Dou, S. X. & Liu, H. K. (2008). *Chem. Asian J.* **3**, 854–861.

Nakamoto K. (1993). *Infrared Spectra of Inorganic and Coordination Compounds*, 4th ed. John Wiley and Sons Inc.

Pan, G.-H., Hayakawa, T., Nogami, M., Hao, Z., Zhang, X., Qu, X. & Zhang, J. (2015). *RSC Adv.* **5**, 88590–88601.

Phanon D. & Gautier-Luneau I. (2010). *Z. Anorg. Allg. Chem* **636**, 2579–2583.

Rau, R. C. (1966). *Acta Cryst.* **20**, 716–723.

Rodríguez-Carvajal, J. (1993). *Physica B*, **192**, 55–69.

Smaldone, R. A., Forgan, R. S., Furukawa, H., Gassensmith, J. J., Slawin, A. M. Z., Yaghi, O. M. & Stoddart, J. F. (2010). *Angew. Chem. Int. Ed.* **49**, 8630–8634.

Spek, A. L. (2009). *Acta Cryst.* D**65**, 148–155.

Sun, Y.-L., Feng, X., Guo, N., Wang, L.-Y., Li, R.-F. & Bai, R.-F. (2016). *Inorg. Chem. Commun.* **67**, 90–94.

Takahashi, K., Yokoyama, S., Matsumoto, T., Cuya Huaman, J. L., Kaneko, H., Piquemal, J.-Y., Miyamura, H. & Balachandran, J. (2016). *New J. Chem.* **40**, 8632–8642.

Takase, K., Nishizawa, H., Onda, A., Yanagisawa, K. & Yin, S. (2017). *J. Asian Ceram. Soc.* **5**, 482–488.

Wasson, R., Hall, J. W. & Santiago, B. G. (2009). 61st American Chemical Society Southeast Regional Meeting, 21–24 October 2009, San Juan, Puerto Rico.

Willmott, P. R. *et al.* (2013). *J. Synchrotron Rad.* **20**, 667–682.

Yu, H.-K., Eun, T.-H., Yi, G.-R. & Yang, S.-M. (2007). *J. Colloid Interface Sci.* **316**, 175–182.

Zhang, C., Sun, L., Yan, Y., Shi, H., Wang, B., Liang, Z. & Li, J. (2017). *J. Mater. Chem C*, **5**, 8999–9004.